Segmentation of the Whole Breast from Low-dose Chest CT Images

Shuang Liu*[a], Mary Salvatore[b], David F. Yankelevitz[b], Claudia I. Henschke[b] and Anthony P. Reeves[a]

[a]School of Electrical and Computer Engineering, Cornell University, Ithaca, NY, USA
[b]Departments of Radiology, Mount Sinai School of Medicine, New York, NY, USA

ABSTRACT

The segmentation of whole breast serves as the first step towards automated breast lesion detection. It is also necessary for automatically assessing the breast density, which is considered to be an important risk factor for breast cancer. In this paper we present a fully automated algorithm to segment the whole breast in low-dose chest CT images (LDCT), which has been recommended as an annual lung cancer screening test. The automated whole breast segmentation and potential breast density readings as well as lesion detection in LDCT will provide useful information for women who have received LDCT screening, especially the ones who have not undergone mammographic screening, by providing them additional risk indicators for breast cancer with no additional radiation exposure. The two main challenges to be addressed are significant range of variations in terms of the shape and location of the breast in LDCT and the separation of pectoral muscles from the glandular tissues. The presented algorithm achieves robust whole breast segmentation using an anatomy directed rule-based method. The evaluation is performed on 20 LDCT scans by comparing the segmentation with ground truth manually annotated by a radiologist on one axial slice and two sagittal slices for each scan. The resulting average Dice coefficient is 0.880 with a standard deviation of 0.058, demonstrating that the automated segmentation algorithm achieves results consistent with manual annotations of a radiologist.

Keywords: Whole breast segmentation, breast density, low-dose CT images, fully automated segmentation

1. INTRODUCTION

Breast cancer screening with mammogram has been recommended by the United States Preventive Services Task Force (USPSTF) and American Cancer Society and been proven to decrease the mortality from breast cancers. Recent studies suggest that 3D imaging modalities such as breast tomosynthesis[1] and chest CT[2] can also be helpful for breast cancer screening by demonstrating that breast density readings on 3D modalities are consistent with readings on 2D mammogram with greater inter-observer agreement.

The segmentation of the whole breast serves as the first step towards automated detection of breast lesions and automated assessment of breast density, which is considered to be an important risk factor for breast cancer. A fully automated algorithm to segment the whole breast in LDCT is presented in this paper. LDCT has been recently recommended by USPSTF as an annual lung cancer screening test for older smokers. The automated whole breast segmentation and potential breast density readings as well as lesion detection will provide useful information for women who have received LDCT screening, especially the ones who have not undergone mammographic screening, by providing them additional risk indicators for breast cancer with no additional radiation exposure.
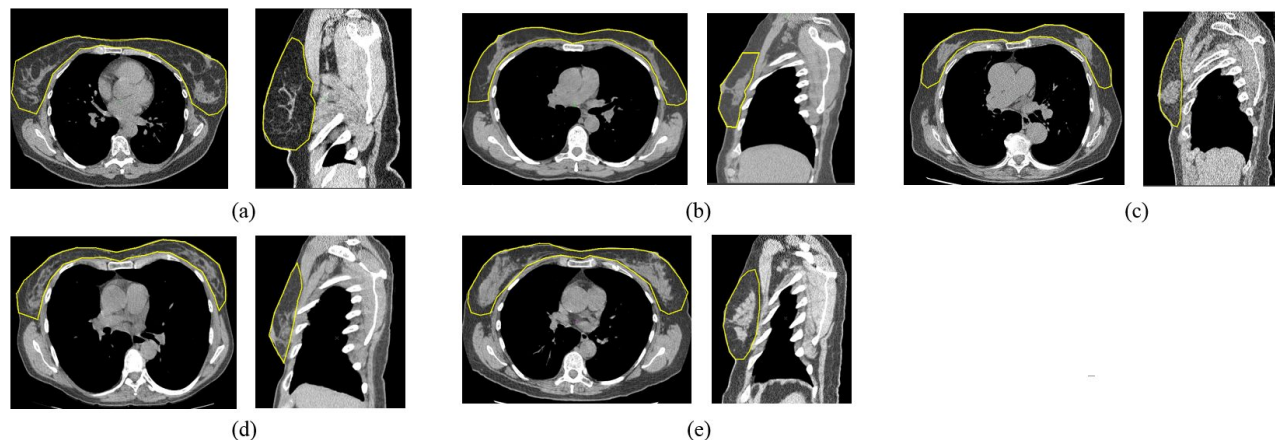
Figure 1. Five examples of breast region with ground truth annotated (indicated by yellow contours) by a radiologist. For each case, both an axial slice and a sagittal slice of the left breast are shown. It can be seen that there is a large range of individual variations of breasts.
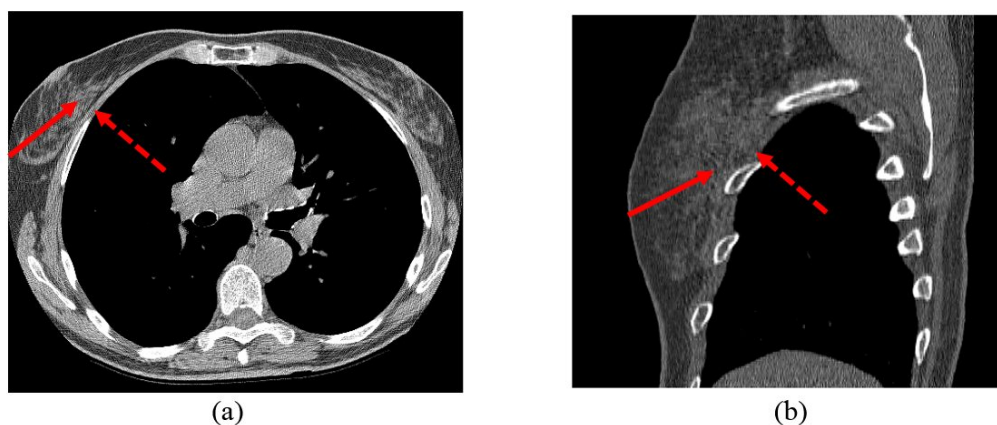

Figure 2. CT (a) axial slice and (b) sagittal slice. Solid arrows mark glandular tissues in the breast and dashed arrows mark the muscles in the pectoral regions.

There are two main challenges to the automated segmentation of the whole breast in LDCT. First, the algorithm must accommodate a significant range of individual variations in terms of size, shape, location and tissue compositions of the breasts as illustrated in Figure 1. LDCT scans are usually taken in the supine positions, while other modalities such as mammogram, dedicated breast CT, and breast MRI acquire images either in the prone position or with breast compression to constrain the location and shape of the breasts. As a result, there is a much greater range of variations in terms of shape and location of the breast in LDCT images than in images of other modalities. Second, glandular tissues located in the posterior breast regions may be difficult to be distinguished from the surrounding muscles in the pectoral regions as illustrated by arrows in Figure 2, because they have similar CT intensity distributions and can be in contact with each other, thereby lacking in well-defined boundaries to exclude the muscles from the breast regions. Moreover, the glandular tissues usually have irregular shapes, which complicates the task of separating glandular tissues and muscles.

There has been considerable interest in algorithm development for segmenting the whole breast in other imaging modalities, but no published work has been found to focus specifically on LDCT. Methods developed for other imaging modalities or standard-dose CT do not translate well to LDCT due to the high levels of noise in the low-dose scans. Atlas based approaches[3, 4] have been used to segment the whole breast region in CT images. In contrast, our work focuses on robust whole breast segmentation using an anatomy directed rule-based method that does not rely on a manually generated atlas. The presented algorithm depends on the segmentation of several organs and tissues that is

provided by our previous studies, which include skin and fat segmentation[7], rib segmentation[5], sternum segmentation[6] and lung segmentation[9].

2. ALGORITHM

The human breast is located outside the thoracic cavity and lies on the underlying muscles, which consist of two major types as shown in Figure 3: (1). Anterior muscles M_A lying on the thoracic wall such as pectoralis major muscle and intercostal muscles; (2). Posterior muscles M_P attached to scapula such as latissimus dorsi muscle and teres major muscle. The whole breast B is defined in this paper as the region including the complete mammary glands G and excluding any muscle tissues (i.e., M_A and M_P). The segmentation of the whole breast requires the determination of the vertical extents, lateral extents, anterior extents and the posterior extents of the breast region. The presented algorithm consists of the following four main steps with the flow chart shown in Figure 4:

1. Identify the anterior and lateral extents using skin segmentation S.
2. Separate the whole breast B from the posterior muscles M_P.
3. Separate the whole breast B from the anterior muscles M_A.
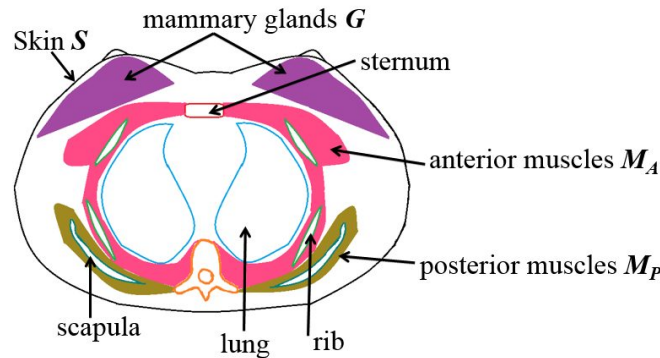4. Determine the vertical extents based on the location of the sternal angle and the inferior end of the sternum.

Figure 3. Human tissues and organs in the chest region shown in an axial view.

2.1 Anterior and lateral extent identification

The whole breast region B is constrained by the skin surface S as shown in Figure 3. Therefore, the lateral extents and anterior extents of B are identified using the skin surface, which is segmented in our previous work[7] as illustrated in Figure 4 (b). If we let R denote the region of interest, which will be further constrained by the subsequent steps using posterior and vertical extents of B and result in the final whole breast segmentation, R is initialized as the interior region constrained by the skin S.

2.2 Separation from the posterior muscles M_P

The posterior extents of the whole breast B consist of two parts: (1). The separation between B and the posterior muscles M_P as illustrated in Figure 4 (c); (2). The separation between B and the anterior muscles M_A as illustrated in Figure 4 (d). The separation from M_P and M_A are determined in this step and the next step respectively, relying on the identification of several tissues and organs, which include the thoracic cavity C, the fat tissues F, and the combined tissues M_G of muscles and mammary glands, in the region of interest R.

The whole breast B is located outside the thoracic cavity C, which is approximated by constructing a convex hull of sternum and ribs (segmented based on previous studies[5, 6]), as shown in Figure 5 (b). The region of interest R is then updated by excluding C as follows:

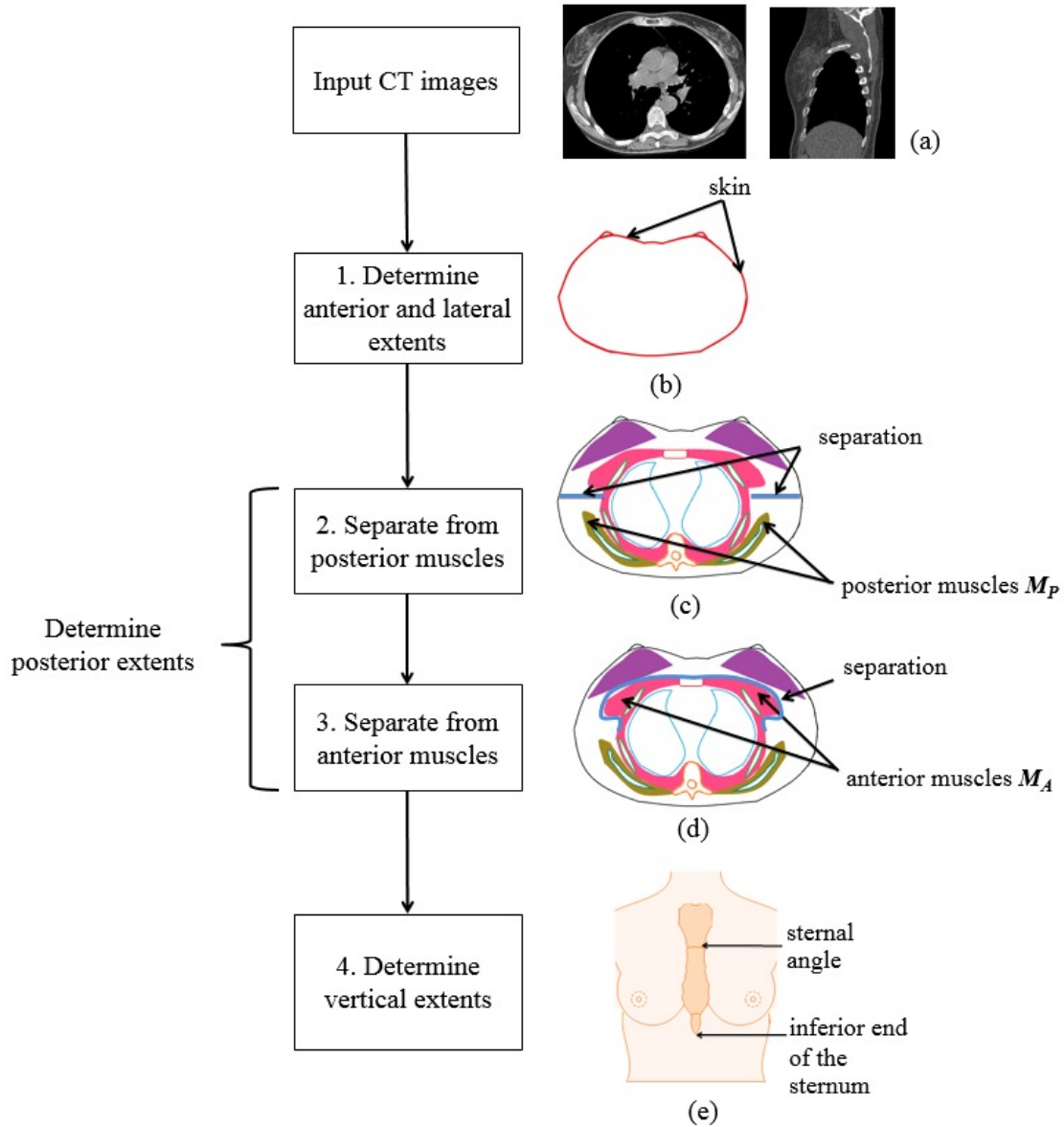$$R \leftarrow R \cap \bar{C} \tag{1}$$

Figure 4. Flow chart of the algorithm with illustrations associated with each step.

There are now two major components contained in the updated R: the fat tissues F and the combined tissues M_G of muscles and mammary glands. Thus, given the fat tissues F segmented using algorithm described in our previous work[7], the combined tissues M_G is obtained as follows:

$$M_G \leftarrow R \cap \bar{F} \qquad (2)$$

As shown in Figure 5 (b), the combined tissues M_G consists of the mammary glands G, the anterior muscles M_A and the posterior muscles M_P, and the separation of B from muscles is equivalent to the distinction of the three components of M_G.
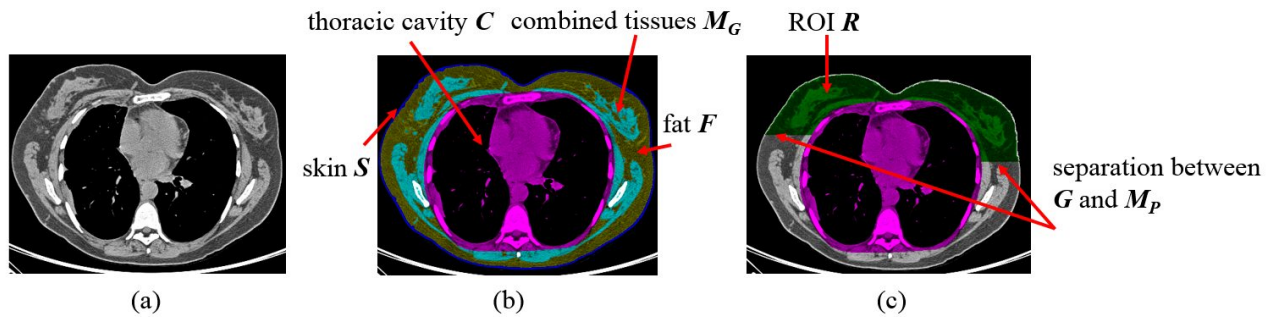
Figure 5. (a) CT axial slice. (b) The identification of the skin S (in blue), thoracic cavity C (in purple), the fat tissues F (in yellow), and the combined tissues M_G (in cyan). (c) The updated region of interest R after determining the separation between G and M_P.
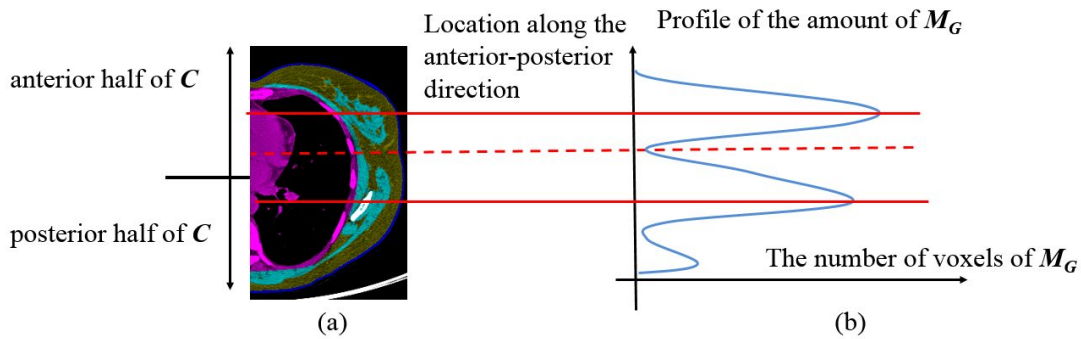

Figure 6. Determination of the separation between mammary glands G (of the left breast) and M_P. (a) The skin S (in blue), thoracic cavity C (in purple), the fat tissues F (in yellow), and the combined tissues M_G (in cyan) of the right breast are shown. (b) The profile of the amount of combined tissues M_G along the anterior-posterior direction.

A gap along medial-lateral direction is usually observed between the mammary glands G and the posterior muscles M_P as shown in Figure 5 (c), which is then considered as the separation between G and M_P. The steps of locating the gap between G and M_P on each axial slice are summarized as follows and illustrated in Figure 6:

1. Construct a profile of the number of M_G voxels on each medial-lateral level with respect to its location along the anterior-posterior direction, as illustrated in Figure 6 (b).
2. Locate the two medial-lateral levels with greatest amount of M_G in the anterior half and posterior half of the thoracic cavity C, respectively, as indicated by solid red solid lines in Figure 6.
3. Determine the medial-lateral level with minimal amount of M_G and located between the two levels determined in the previous step, as indicated by red dashed line in Figure 6.

The left and right breasts are separated from M_P independently using the same algorithm as described above. The division between the left and right breasts is obtained based on the sternum segmentation. For example as shown in Figure 6 (a), when considering the left breast, the algorithm is only applied on the image region right to the sternum. The region of interest R is then updated by excluding the regions posterior to the determined separations as shown in Figure 5 (c) by the green shaded region.

2.3 Separation from the anterior muscles M_A

The region of interest R updated by previous steps contains fat tissues F, mammary glands G, and muscles M_A that is supposed to be excluded from B as shown in Figure 5 (c). An anatomy directed two-stage region growing method is applied on M_G (only the part contained in R) to identify muscles M_A. The first stage is a location-based preliminary growing, which follows the observation that muscles M_A generally lie on the surface of the thoracic cavity C and are separated from the outer mammary glands G by a layer of fat tissues F as shown in Figure 7 (b). The second stage is a rule-based further growing, which enforces a sets of rules to identify muscles that are under-segmented by the first stage.
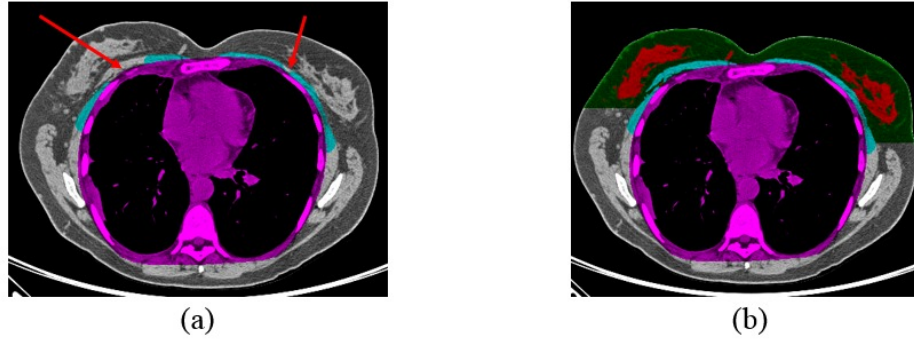
Figure 7. An anatomy directed two-stage region growing method. (a) Muscles M_A (in cyan) identified by the first stage. Arrows point to the muscles that are under-segmented. (b) Results of the second stage growing. The thoracic cavity C (in purple), the mammary glands G (in red), the muscles M_A (in cyan), and updated region of interest R (in green and red) are shown.

Stage 1: Location-based preliminary growing of muscles M_A

It is usually observed that the muscles M_A lie on the surface of the thoracic cavity C and are separated from the outer mammary glands G by a layer of fat tissues F as shown in Figure 7 (b). As a result, the nearest layer of fat to C and the distance between M_G voxels and C are used to identify M_A as follows:

1. Initialize muscles M_A by including voxels located on the boundary of the thoracic cavity C.
2. For each M_A voxel v, compute its 3D Euclidean distance $\lambda(v)$ to the nearest fat F voxel.
3. For each M_A voxel v, include all M_G voxels within the distance $\lambda(v)$ into M_A.

An example of muscles M_A identified after the first stage is shown by the cyan regions in Figure 7 (a). The region of interest R and the combined tissues M_G of interest are then updated as follows:

$$R \leftarrow R \cap \overline{M_A} \qquad (3)$$

$$M_G \leftarrow R \cap M_G \qquad (4)$$

Stage 2: Rule-based further growing of muscles M_A

The underlying assumption of the first stage growing is that there are no fat tissues separating muscles M_A and thoracic cavity C, however, it does not apply to all circumstances, and therefore some muscle voxels may be under-segmented as indicated by arrows in Figure 7 (a). M_A is further grown by enforcing geometry constraint and connectivity constraint sequentially on M_G based on the observation that M_G voxels located near the lung and M_A with high degree of connectivity to M_A are very likely to be muscles. The detailed steps are summarized as follows:

1. On each axial slice, apply 2D connected component labelling on M_G voxels.
2. Identify all candidate muscle components, which are defined as M_G components with lateral distance less than τ mm to the nearest M_A voxels, i.e., τ is a threshold for the lateral thickness of muscles on an axial slice .
3. For each candidate muscle component c, if it is close enough to the lung (segmented in previous study[9]) with high degree of connectivity to M_A voxels, then c is included into M_A. Specifically, let $\lambda(c)$ denote the average 2D Euclidean distance from voxels of c to the lung, and let $d(c)$ denote the degree of connectivity of c to M_A voxels, which is defined as the anterior-posterior span of voxels connected to M_A voxels and located in the anterior region of c. If the component c satisfies any of the following three criteria, then it is included into M_A:
    i. $d(c) > \sigma_1$ and $\lambda(c) < \tau_1$
    ii. $d(c) > \sigma_2$ and $\lambda(c) < \tau_2$
    iii. $d(c) > \sigma_3$ and $\lambda(c) < \tau_3$
Where $0 < \sigma_1 < \sigma_2 < \sigma_3$ and $0 < \tau_1 < \tau_2 < \tau_3$, which reflects the trade-off between the degree connectivity and distance to M_A voxels.

The degree of connectivity $d(c)$ for a muscle component c is defined using only the anterior region (located within 1 mm to the anterior end of c) of c. This is because we observe that both mammary glands and muscles component can be

connected to the M_A voxels identified in the first stage, as illustrated in Figure 8 (a) by dashed arrows. However, only the anterior region of a muscle component is usually connected to M_A, as indicated by the dashed arrow on the left in Figure 8 (a), which is therefore used as the basis to classify candidate muscle components into mammary glands and muscles.
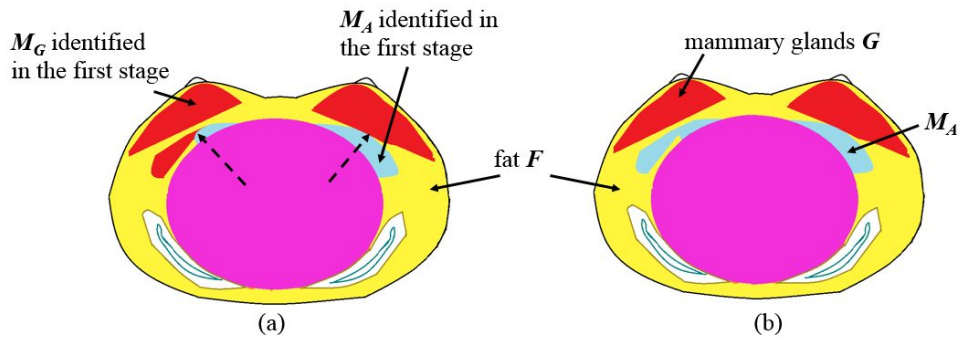

Figure 8. Both mammary glands and muscles component can be connected to the M_A voxels identified in the first stage, as illustrated by dashed arrows. However, only the anterior region of a muscle component is usually connected to M_A, as indicated by the dashed arrow on the left. (a) The tissue compositions determined in the first stage. Updated M_G and M_A are shown in red and cyan respectively. Note that on the left side of the image, some muscles are under-segmented. (b) The real tissue compositions (mammary gland G (in red), muscles M_A (in cyan) and fat F (in yellow)) shown on an axial slice.

An example of muscles M_A identified after the second stage is shown by the cyan regions in Figure 7 (b). The region of interest R and the segmented mammary glands G are then determined as follows:

$$R \leftarrow R \cap \overline{M_A} \tag{5}$$

$$G \leftarrow R \cap M_G \tag{6}$$

2.4 Vertical extent determination

The superior and inferior extents of the breast region B are observed to approximately coincide with the sternal angel A and the inferior end E of the sternum, which are provided by the sternum segmentation[5], as illustrated in Figure 4 (e). Therefore, the vertical span of B is first initialized as the vertical span between A and E, and then is refined to the actual glandular tissue extent as follows:

1. On each axial slice located beyond the initial vertical span, perform 2D connected component labelling on the segmented mammary glands G voxels.
2. To determine the superior extent, starting at the axial level of the sternal angle A, move in the cranial direction and locate the first axial slice with no significant G components.
3. To determine the inferior extent, starting at the axial level of the caudal end E of the sternum, move in the caudal direction and locate the first axial slice with no significant G components.

The whole breast segmentation B is then determined by excluding axial levels beyond the determined vertical span from the region of interest R.

3. EXPERIMENTS

The presented algorithm was evaluated on 20 LDCT images (120kV-140kV, 40mA-80mA) from the LIDC public dataset[8] with slice thickness less than 1.25 mm. The quantitative evaluation is used to validate the presented algorithm. For each CT scan, the ground truth for the whole breast region is manually annotated by a radiologist on one axial slice and two sagittal slices. The axial slice is selected at the axial level intersecting nipples, and the two sagittal slices are selected at the median level of left and right breast respectively as illustrated by Figure 9. Figure 1 also contains examples that are manually annotated and used as ground truth. Dice coefficient (DC), which is defined as twice the intersection area divided by the sum of the individual areas, is used to measure the agreement between the automated segmentation and the ground truth.
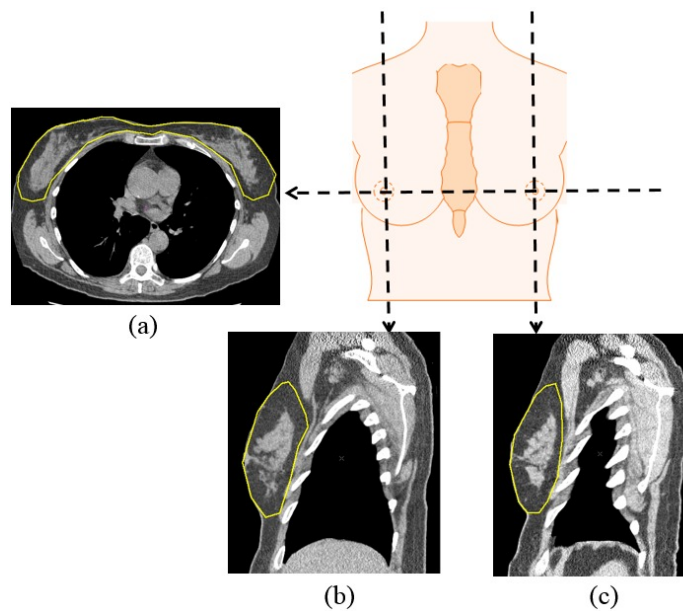
Figure 9. Example of ground truth (indicated by yellow contours) annotated by a radiologist on (a) one axial slice and (b, c) two sagittal slices for one CT scan.

4. RESULTS

Examples of segmentation outcomes are shown in Figure 10 (a-c) as 3D visualizations and (d-f) their respective 2D axial visualizations. For the 3D visualizations, the sternum and the segmented mammary glands G are also shown as reference. For the 2D axial visualizations, the thoracic cavity C, the segmented mammary glands G and anterior muscles M_A are also shown as reference.

The quantitative evaluation results for 20 scans (20 axial annotations and 40 sagittal annotations) are summarized in Table 1. An overall mean Dice coefficient of 0.880 with standard deviation of 0.058 is achieved.

Table 1. Dice coefficients (DC) for axial annotations, sagittal annotations and overall annotations.

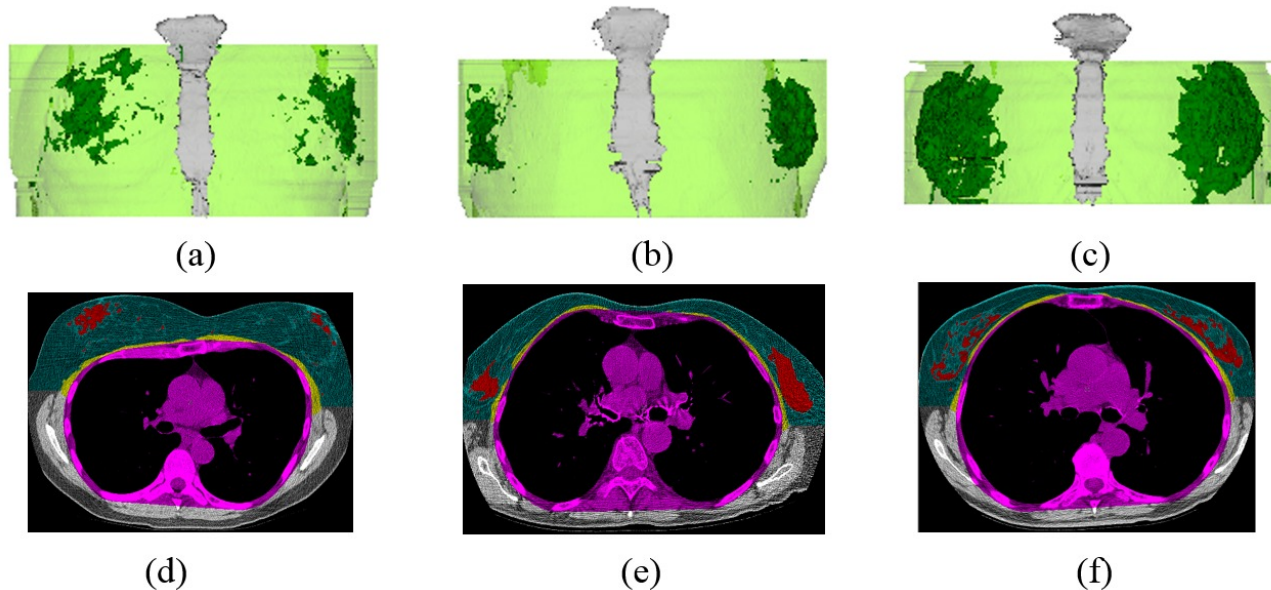|	Mean DC	Max DC	Min DC	Standard deviation
Axial (20 slices)	0.930	0.962	0.867	0.024
Sagittal (40 slices)	0.830	0.880	0.758	0.033
Overall (60 slices)	0.880	0.962	0.758	0.058

Figure 10. (a-c) 3D coronal visualizations of the whole breast segmentation (in light green) from three different CT scans. The segmentation of sternum (in grey) and the mammary glands (in dark green) are also shown as reference. (d-f) 2D axial visualization of the whole breast segmentation (in blue) for respective scans in the first row. The mammary glands G (in red), the muscles M_A (in yellow), and the thoracic cavity C (in purple) are also shown as reference.

5. DISCUSSION

The evaluation results report a mean DC on axial slices of 0.930, which indicates a satisfactory determination of lateral, anterior, and posterior extents. The mean DC of 0.830 on sagittal slices is not as encouraging as that on axial slices, thereby suggesting that the automatically determined vertical extents generally differ from the manually annotated extents. The challenge of determining vertical extents stems from the lack of well-defined superior and inferior breast boundaries. Examples of segmentation results are shown in Figure 11 and arranged from left to right in the order of decreasing DC. The original CT images and the comparison between the segmentation and the manual annotations are shown in the axial view and sagittal view respectively. Correct segmentation is in red, over-segmentation is in green and under-segmentation is in purple. The under-segmentation of breast regions on sagittal slices is common as indicated by the purple regions in Figure 11 (h, j, l) and thus results in low DC. However, although cases as shown in Figure 11 (j, l) have relatively low DC, the complete mammary glands are successfully segmented and most of the muscles are excluded, in which case the under-segmentation will not influence the potential breast lesion analysis in the future.

The vertical span of the whole breast region is determined based on the sternal angle and the inferior end of the sternum, rather than the actual vertical extents of mammary glands G segmented in section 2.3. This is because G tends to be over-segmented at the axial levels superior to the sternal angle, i.e., the muscles M_A may not be completely identified in the third step of the algorithm, due to two main reasons as illustrated in Figure 12. First, the level of image noise is usually higher at the superior axial levels due to the existence of shoulder bones, thereby making it more challenging for the automated algorithm to perform well. Second, the shape, geometry and dimensions of the muscles at the axial levels superior to the sternal angle differ significantly from those at axial levels of the breast region as indicated by arrows in Figure 12. As a result, the assumptions and constrains suitable for identifying muscles in the breast regions do not translate well in the region superior to the breast region. On the other hand, we observed that the sternum provides decent references for determining the vertical span of the breast region, and further refinement based on the actual glandular tissues location is good enough to result in a satisfactory outcome.
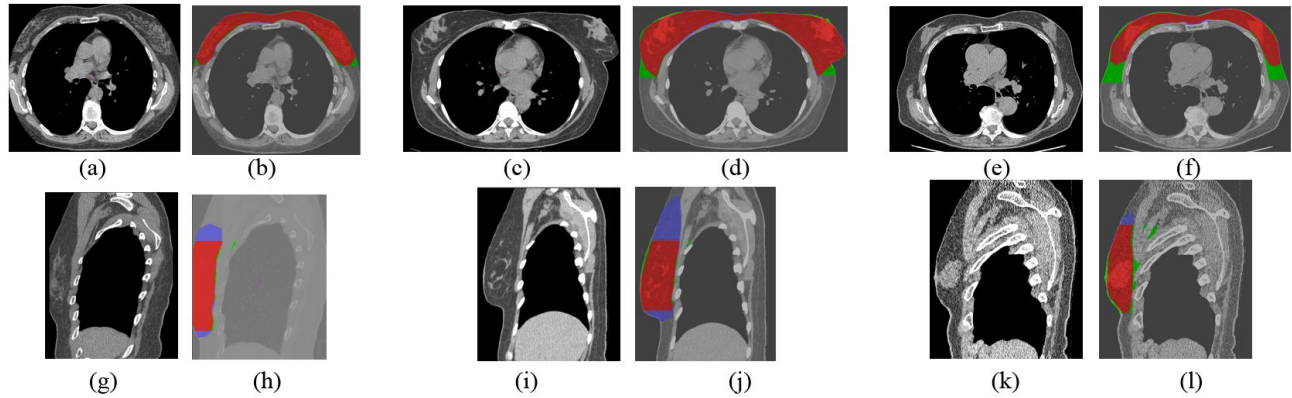
Figure 11. Examples of segmentation are arranged from left to right in the order of decreasing DC. (a, c, e, g, i, k) are the original CT slices, and (b, d, f, h, j, l) are the segmentation compared to the ground truth for respective cases. Correct segmentation is in red, over-segmentation is in green and under-segmentation is in purple. The DC for (a-f) axial slices are 0.962, 0.951, 0.867 respectively, and for (g-l) sagittal slices is 0.880, 0.805 and 0.758 respectively.
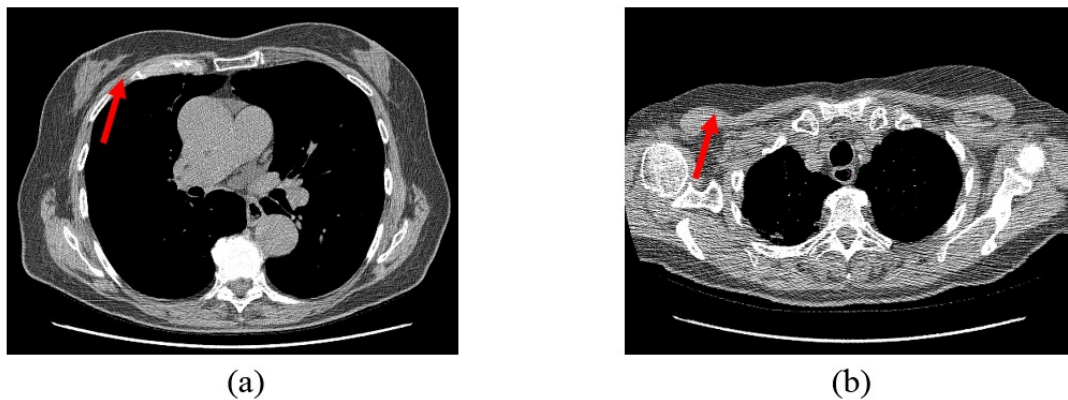

Figure 12. Axial CT slices at (a) the median level of the breast and at (b) the level superior to the sternal angle. The arrows indicate significant variations in terms of the shape and dimensions of muscles at these two axial levels.

In future work we plan to quantitatively validate the segmentation of the glandular tissue and to analyze the geometry of the glandular tissue to identify breast abnormalities. In addition, we plan to quantitatively evaluate the utility of the ratio of the volume of glandular tissues to that of the whole breast for the fully automated measurement of breast density.

6. CONCLUSION

The segmentation of whole breast is necessary for automatically assessing the breast density and serves as the first step towards automated breast lesions detection. A fully automated algorithm to segment the whole breast in LDCT has been presented in this paper. Segmentation of 20 LDCT scans was evaluated by comparing to manually annotated ground truth. The resulting average Dice coefficient is 0.880 with a standard deviation of 0.058, demonstrating that the automated segmentation algorithm achieves results consistent with manual annotations of a radiologist.

ACKNOWLEDGMENTS

REFERENCES

[1] Bakic, P. R., Carton, A. K., Kontos, D., Zhang, C., et al., "Breast percent density: estimation on digital mammograms and central tomosynthesis projections," Radiology 252(1), 40-49 (2009).

[2] Salvatore, M., Margolies, L., Kale, M., Wisnivesky, J., et al., "Breast Density: Comparison of Chest CT with Mammography," Radiology 270(1), 67-73 (2014).

[3] Zhou, X., Han, M., Hara, T., Fujita, H., et al., "Automated segmentation of mammary gland regions in non-contrast X-ray CT images," Computerized Medical Imaging and Graphics 32(8), 699-709 (2008).

[4] Reed, V. K., Woodward, W. A., Zhang, L., Strom, E. A., et al., "Automatic segmentation of whole breast using atlas approach and deformable image registration," International journal of radiation oncology, biology, physics 73(5), 1493-1500 (2009).

[5] Liu, S., Xie Y., and Reeves, A.P., "Segmentation of the sternum from low-dose chest CT," Proc. SPIE (TBA), Accepted (2015).

[6] Lee, J. and Reeves, A.P., "Segmentation of individual ribs from low-dose chest CT," Proc. SPIE 7624, 76243J (2010).

[7] Padegett, J., Biancardi, A. M., Henschke, C. I., Yankelevitz, D. F., et al., "Local noise estimation in low-dose chest CT images," International journal of computer assisted radiology and surgery 9(2), 221-229 (2014).

[8] Reeves, A. P., Biancardi, A. M., Apanasovich, T. V., Meyer, C. R., et al., "The lung image database consortium (LIDC) a comparison of different size metrics for pulmonary nodule measurements," Academic radiology 14(12), 1475-1485 (2007).

[9] Reeves, A. P., Chan, A. B., Yankelevitz, D. F., Henschke, C. I., et al., "On measuring the change in size of pulmonary nodules," IEEE Transactions on Medical Imaging 25(4), 435-450 (2006)